Active matter at high density: Velocity distribution and kinetic temperature ⊘

Lorenzo Caprini ✉ ⓘ ; Umberto Marini Bettolo Marconi ⓘ

Check for updates

View Online

Export Citation

02 May 2024 12:26:31

Boost Your Optics and
Photonics Measurements

Lock-in Amplifier

Zurich
Instruments

Find out more

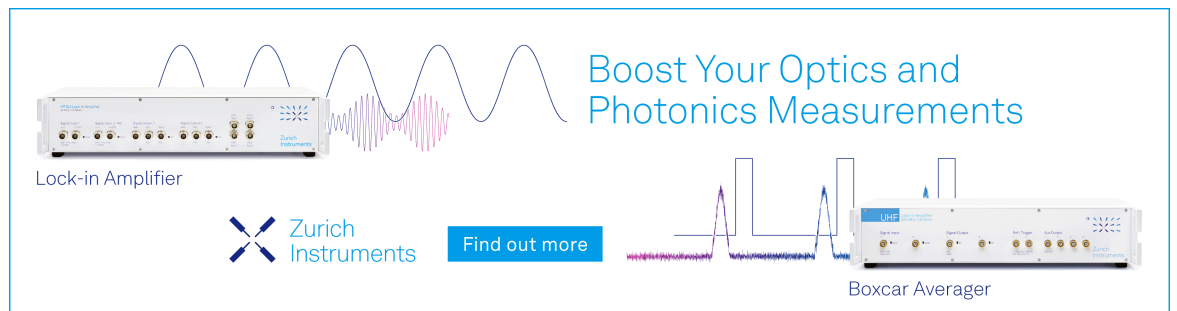Boxcar Averager

Active matter at high density: Velocity distribution and kinetic temperature

View Online   Export Citation   CrossMark

Lorenzo Caprini[a] 🆔 and Umberto Marini Bettolo Marconi 🆔

AFFILIATIONS

Dipartimento di Fisica, Universitá di Camerino, Via Madonna delle Carceri, I-62032 Camerino, Italy

[a]Author to whom correspondence should be addressed: lorenzo.caprini@gssi.it

ABSTRACT

We consider the solid or hexatic non-equilibrium phases of an interacting two-dimensional system of active Brownian particles at high density and investigate numerically and theoretically the properties of the velocity distribution function and the associated kinetic temperature. We obtain approximate analytical predictions for the shape of the velocity distribution and find a transition from a Mexican-hat-like to a Gaussian-like distribution as the persistence time of the active force changes from the small to the large persistence regime. Through a detailed numerical and theoretical analysis of the single-particle velocity variance, we report an exact analytical expression for the kinetic temperature of dense spherical self-propelled particles that holds also in the non-equilibrium regimes with large persistence times and discuss its range of validity.

Published under license by AIP Publishing. https://doi.org/10.1063/5.0029710

I. INTRODUCTION

Active matter at high density is becoming a subject of great interest since it plays a crucial role to understand a broad range of biological systems,[1–4] such as bacterial colonies[5–7] and cell monolayers.[8] Experimental observations realized with cell monolayers reveal large-scale collective motion, such as swirls and velocity alignment.[8–12] In the spirit of minimal modeling, these systems have been recently modeled using high-density interacting Active Brownian Particles (ABPs),[8,13] thus modeling the complex cells and cell–substrate interactions through steric interaction and self-propulsion. Depending on their density, interacting systems of ABP display a variegate phenomenology. In particular, at moderate packing fractions, a non-equilibrium phase-coexistence known as Motility-Induce Phase-Separation (MIPS)[14–18] occurs even in the absence of attractive interactions.[19–28] Depending on the active force and the packing fraction, ABP can also attain homogeneous configurations, such as active liquid, hexatic, and solid phases.[29–35] With respect to equilibrium systems of Brownian colloids, the active liquid–hexatic and hexatic–solid transitions are shifted toward larger values of the packing fractions, and the hexatic phase occurs for a broad range of parameters.[33,36–38] Moreover, the dense phases of interacting ABP display a plethora of dynamical phenomena, making them quite different as compared to passive dense phases. In particular, the particle velocities spontaneously form ordered domains even in the absence of explicit alignment interactions in phase-separated configurations[19] and in active liquid, hexatic, and solid phases[38] and give rise to fascinating intermittency phenomena.[38,39] The spontaneous alignment mechanism makes the ABP models suitable to describe the behavior of cell monolayers.

For systems of interacting ABP, several authors, searching for an extension of equilibrium thermodynamic concepts, introduced an effective "temperature" in the study of non-equilibrium systems of self-propelled particles. Following ideas from glassy systems, several authors introduce the dynamical effective temperature by the ratio between the mean-square-displacement and the time-integrated linear response function due to small perturbation, in the context of active disks,[40–49] dumbbells,[50,51] and polymers,[52] looking both at active homogeneous (liquid, hexatic, and solid) configurations and phase-separated regimes. In the homogeneous case, the effective temperature increases as the propulsive speed increases and decreases as the packing fraction grows. Instead, in the inhomogeneous case, i.e., when MIPS occurs, the net distinction between the populations of the two coexistent phases, e.g., slow particles in the dense clusters and fast particles in the disordered phase, allows us to introduce two distinct effective temperatures.[49] Mandal *et al.*[53] focused on the kinetic temperature, i.e., the variance of the velocity distribution, for underdamped self-propelled particles, outlining

that the temperatures in the two coexisting phases of MIPS are different. An alternative definition of the active temperature has been also proposed in the context of stochastic thermodynamics to generalize the Clausius relation to active systems, a program requiring the introduction of a space-dependent temperature that depends on the potential itself.[54–56]

In this work, we shall not discuss the concept of temperature in non-equilibrium active systems,[57] intended as an observable satisfying well-defined thermodynamic relations, an issue still a matter of debate, but focus on the kinetic temperature of self-propelled particles. We find its exact analytical expression as a function of the model parameters for dense homogeneous configurations in the non-equilibrium active solid and hexatic phases. We also obtain the ABP single-particle velocity distribution in these highly packed configurations as the persistence time of the self-propulsion varies. The shape of this distribution obtained via numerical simulations is compared with theoretical predictions both in the small and the large persistence regimes. We find a crossover between the two regimes that manifests itself in a qualitative change in the shape of the velocity distribution.

This manuscript is organized as follows: in Sec. II, we introduce the model, while in Sec. III, we report the velocity dynamics representing the starting point of our theoretical approach. Numerical and theoretical results of single-particle velocity distributions are shown in Sec. IV, while the analysis of the first moments of the distribution and the discussion about the kinetic temperature are reported in Sec. V. Finally, we report some discussions and conclusions in the Sec. VI.

II. INTERACTING SELF-PROPELLED PARTICLES

We consider a two-dimensional system of N self-propelled disks, described by the Active Brownian Particle (ABP) model, where inertial and hydrodynamic effects are neglected. The position, $\mathbf{x}_i$, of each disk evolves by the following stochastic differential equation:

$$\gamma \dot{\mathbf{x}}_i = \mathbf{F}_i + \mathbf{f}_i^a. \qquad (1)$$

The constant γ is the solvent friction coefficient while the stochastic force associated with the thermal agitation of the solvent has been neglected. Indeed, for several experimental active particle systems,[1] the thermal diffusivity is some orders of magnitude smaller than the diffusivity associated with the self-propulsion force, $\mathbf{f}_i^a$. According to the popular ABP model, $\mathbf{f}_i^a$ is a time-dependent force given by the following equation:

$$\mathbf{f}_i^a = \gamma v_0 \mathbf{n}_i, \qquad (2)$$

where v_0 is the constant modulus of the swim velocity induced by $\mathbf{f}_i^a$ and $\mathbf{n}_i$ is the orientation vector of components $(\cos\theta_i, \sin\theta_i)$ evolving through a stochastic process. In particular, the orientational angle, θ_i, performs angular diffusion,

$$\dot{\theta}_i = \sqrt{2D_r}\,\xi_i, \qquad (3)$$

where ξ_i is a white noise with unit variance and zero average and D_r is the rotational diffusion coefficient. We remark that the inverse of D_r defines the correlation-time of the active force, namely, $\tau = 1/D_r$,[58] which will be assumed as a control parameter in the numerical study performed in this manuscript.

The term $\mathbf{F}_i$ represents the repulsive force between particles due to steric interactions. In particular, $\mathbf{F}_i = -\nabla_i U_{tot}$ where the potential, U_{tot}, can be expressed as $U_{tot} = \sum_{i<j} U(|\mathbf{x}_{ij}|)$, with $\mathbf{x}_{ij} = \mathbf{x}_i - \mathbf{x}_j$. We choose $U(r)$ as a shifted, truncated Lennard Jones potential as follows:[19,59]

$$U(r) = 4\epsilon\left[\left(\frac{\sigma}{r}\right)^{12} - \left(\frac{\sigma}{r}\right)^{6}\right] + \epsilon, \qquad r \le 2^{1/6}\sigma \qquad (4)$$

and zero for $r > 2^{1/6}\sigma$. The constant ϵ is the typical energy scale of the interactions, while σ is the nominal particle diameter. The short-range nature of the potential allows us to consider only the force contributions of first-neighboring particles even in the very packed configurations considered in this paper. Both ϵ and σ are set to one for numerical convenience.

We focus on high density regimes exploring the homogeneous aggregation phases of self-propelled particles. In particular, we fix $v_0 = 50$ and the packing fraction, $\phi = N/L^2\sigma^2/4$, to the value 1.1, where the system attains active solid or hexatic configurations without showing density inhomogeneities.[38] In particular, the hexatic–solid transition is controlled by τ and occurs approximatively at $\tau = 0.1$. Under these conditions, we study the single-particle velocity distribution varying τ and its moments. We can distinguish between two regimes:[38] (i) the small persistence regime where $\tau < U''(\bar{r})/\gamma$ and (ii) the large persistence regime where $\tau > U''(\bar{r})/\gamma$, with $\bar{r}$ being the average distance between neighboring particles that is fixed by the density in any homogeneous configurations. In case (i), the self-propulsion $\mathbf{f}_i^a$ is the fastest degree of freedom: in this regime, the persistence time, τ, is smaller than the typical time of the potential $U''(\bar{r})/\gamma$ so that the behavior of ABP resembles that of passive Brownian particles and $\mathbf{x}_i$ just display oscillations around their equilibrium positions. Considering the structural properties of the system, this regime is indistinguishable from the passive solid-state. In case (ii), the evolution of $\mathbf{f}_i^a$ plays a relevant role and affects the dynamics of $\mathbf{x}_i$, manifesting itself in several dynamical anomalies[19,38] due to the intrinsic non-equilibrium nature of active models.

III. THE VELOCITY DYNAMICS

As already reported in Refs. 19, 38, and 60, the study of the velocity dynamics reveals the existence of hidden collective behavior of self-propelled particles at high density in the regime of large persistence times. Nevertheless, many single-particle properties, such as the velocity distribution and its moments, have not been yet explored.

Following Ref. 19, we eliminate $\mathbf{f}_i^a$ in favor of $\mathbf{v}_i = \dot{\mathbf{x}}_i$, i.e., the velocity of the particle, which does not coincide with the swim velocity, $v_0\mathbf{n}_i$, since the modulus of $\mathbf{v}_i$ is not fixed and its orientation is not parallel to $\mathbf{n}_i$. This statement is true when particles interact and, thus, at high densities, in particular. Transforming the dynamics from the variables $(\mathbf{x}_i, \mathbf{f}_i^a)$ to the new variables $(\mathbf{x}_i, \mathbf{v}_i)$ (without any approximations), the equations of motion read

$$\dot{\mathbf{x}}_i = \mathbf{v}_i, \qquad (5a)$$

$$\tau\gamma\dot{\mathbf{v}}_i = -\gamma\sum_{j=1}^{N}\mathbf{\Gamma}_{ij}(\mathbf{x}_i - \mathbf{x}_j)\mathbf{v}_j + \mathbf{F}_i + \tau\gamma\mathbf{k}_i, \qquad (5b)$$

where each $\mathbf{\Gamma}_{ij}$ is two-dimensional matrix with components

02 May 2024 12:26:31

$$\Gamma_{ij}^{\alpha\beta}(\mathbf{r}_{ij}) = \delta_{ij}\delta_{\alpha\beta} + \frac{\tau}{\gamma}\nabla_{i\alpha}\nabla_{j\beta}U(|\mathbf{r}_{ij}|). \qquad (6)$$

Greek indices are used to denote the spatial components α, $\beta = x$, y, while Latin indices identify the particle number i, $j = 1, \ldots, N$. Finally, the term $\mathbf{k}_i$ is a noise vector that reads

$$\mathbf{k}_i = v_0\sqrt{\frac{2}{\tau}}\,\boldsymbol{\xi}_i \times \frac{\gamma\mathbf{v}_i + \nabla_i U_{tot}}{\gamma v_0}, \qquad (7)$$

where $\boldsymbol{\xi}_i$ is a vector with components $(0, 0, \xi_i)$ and normal to the plane of motion, $(x, y, 0)$. The vector $\mathbf{k}_i$ is a multiplicative noise depending both on $\mathbf{v}_i$ and $\mathbf{F}_i$ and is perpendicular to $\mathbf{n}_i$, i.e., the orientation of the active force. Its amplitude scales simply as $\sim v_0\sqrt{2/\tau}$ since $\mathbf{n}_i$ is a unit vector.

The dynamics (5b) resembles the evolution of underdamped passive particles that are out from equilibrium because of the occurrence of space-dependent friction forces (e.g., the diagonal terms of the matrix $\boldsymbol{\Gamma}$) and effective forces depending on positions and velocities of neighboring particles (e.g., the non-diagonal terms of $\boldsymbol{\Gamma}$). Equation (5b) resembles the dynamics of the Active Ornstein–Uhlenbeck particle (AOUP),[61–68] an alternative model used to study the behavior of self-propelled particles, such as the accumulation near walls[63,69,70] and MIPS.[71,72] Upon a suitable mapping of the self-propulsion parameters,[73,74] the difference between AOUP and ABP dynamics is represented by the noise term $\mathbf{k}_i$, which in the former is a white noise vector with independent components.[61,71]

IV. PROBABILITY DISTRIBUTION FUNCTION OF THE VELOCITY

We numerically study the distribution of the velocity in the steady-state to evaluate the effect of the persistence time, τ. As illustrated in Figs. 1(a) and 1(b), the distinction between large and small persistence regimes produces different shapes in the probability distribution function of the velocity, $p(v_x, v_y)$. In the small-τ configurations shown in panel (a) [case (i)], $p(v_x, v_y)$ has a pronounced non-Gaussian shape: the probability of finding a particle with $v \approx 0$ is negligible, and the velocity of the particles is peaked around a circular crown with radius $\approx v_0$. Instead, in the large-τ configurations reported in panel (b) [case (ii)], $p(v_x, v_y)$ presents a Gaussian-like shape quite similar to the case of passive Brownian particles. Intuitively, in case (i), the self-propulsion changes rapidly without producing any appreciable change in the particle positions giving rise only to very small fluctuations. The net steric force exerted by the neighboring particles on a tagged particle almost cancels out and has a little effect on the particle velocity that, in practice, only experiences the influence of the active force. This explains why the distribution of $\mathbf{v}$ is very similar to the one of $\mathbf{f}^a$. On the contrary, in the large τ regime, this is no longer true. The direction of the active force before appreciably changing need an interval $\sim\tau$ much larger than the relaxation time associated with the interparticle potential, $\tau_p = U''(\bar{r})/\gamma$. Now, the resultant of the active and steric forces nearly vanishes, and [see Eq. (1)] as a consequence, the average velocity is almost zero and the single-particle kinetic energy decreases.
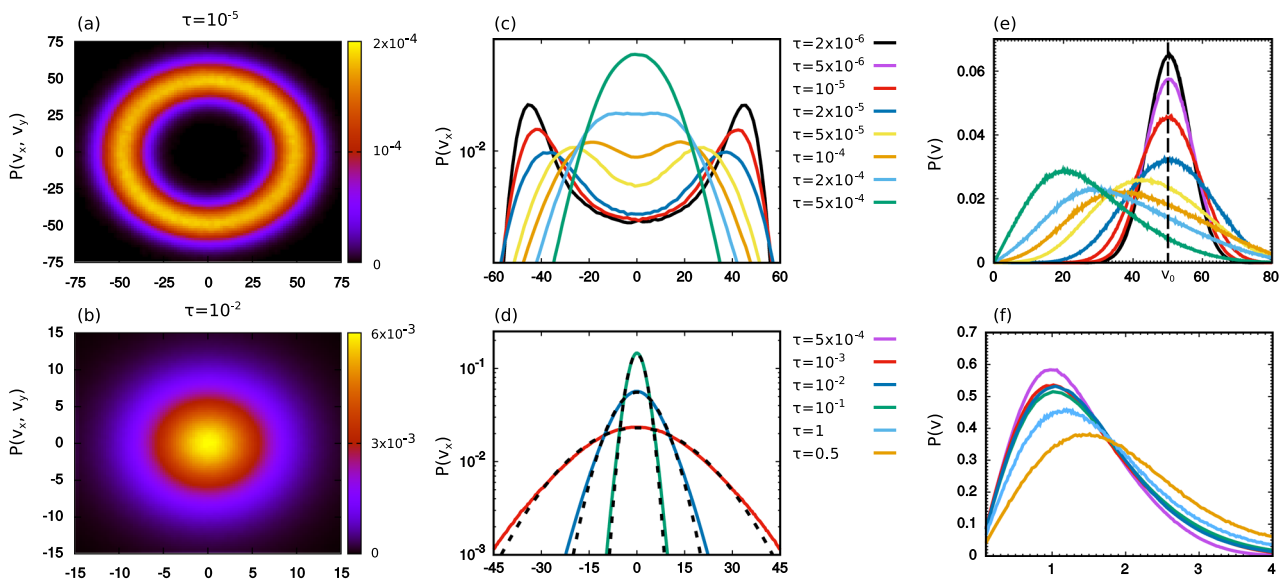
FIG. 1. Probability distribution of the velocity. Panels (a) and (b): map of the two-dimensional probability distribution function, $p(v_x, v_y)$, for two different values of $\tau = 10^{-5}$ [panel (a)] and $\tau = 10^{-2}$ [panel (b)]. Panels (c) and (d): marginal probability distribution function, $p(v_x)$, for several values of τ (colored lines). The dashed black lines in panel (d) are obtained by numerical fits, obtained with Gaussian distributions. Panels (e) and (f): probability distribution of the velocity modulus, $p(|\mathbf{v}| = v)$, for different values of τ. In particular, in panel (f), v is rescaled by τ so that $v \to v\tau^{2/5}$, showing the collapse of the $p(v)$. Panels (c) and (e), and (d) and (f) share the captions. Numerical simulations are obtained with $v_0 = 50$, $\varepsilon = \sigma = 1 = \gamma = 1$.

The transition from regime (i) to regime (ii) is quantitatively evaluated in Figs. 1(c) and 1(d) where the marginal probability distribution of the velocity along one component, $p(v_x) = \int dv_y p(v_x, v_y)$, is studied for different values of τ. For smaller values of τ, $p(v_x)$ displays two symmetric peaks near $v_x \approx v_0$. When τ grows, the peaks shift toward smaller values of v_x and their heights decrease with respect to the $p(v_x)$ value around the origin. For $\tau \gtrsim 2 \times 10^{-4}$, the two peaks merge and the bimodality of the distribution is suppressed, while for further τ-values, a single pronounced peak placed at $v_x \approx 0$ occurs. The deviation between $p(v_x)$ and a Gaussian distribution is not very pronounced as revealed in Fig. 1(d), as shown by the comparison with the best Gaussian fit. To provide another perspective, we study the probability distribution of the velocity modulus, $p(v = |\mathbf{v}|)$, in Figs. 1(e) and 1(f). In the small-τ regime [panel (e)], the distribution is peaked around $v = v_0$ displaying a quite symmetric shape fairly described by a Gaussian centered in $v = v_0$,

$$p(v) \approx \mathcal{N} v \exp\left[-\frac{\alpha}{2}(v - v_0)^2\right], \tag{8}$$

where $\mathcal{N}$ is a normalization factor and α is a parameter. We observe that $p(v)$ becomes narrow as τ grows, in the small-τ regime, but for further values of τ, the peak of the distribution shifts toward smaller values. After a crossover regime, occurring for intermediate values of τ, the distribution $p(v)$ approaches a Gaussian-like shape such that

$$p(v) \approx v \exp\left(-v^2/\beta\right), \tag{9}$$

where $1/\beta = \langle v^2 \rangle$, consistently with the observations of panel (d) of Fig. 1. Interestingly, in panel (f) of Fig. 1, we show that the v-distribution collapses for $v \to v\tau^{2/5}$ for a large range of τ between $(10^{-3}, 10^{-1})$. Thus, $1/\beta$, which plays the role of an effective temperature, decreases as τ is enlarged. We remark that the scaling of $p(v)$ ceases to hold for values $\tau \gtrsim 10^{-1}$ when the homogeneous active solid phase breaks down. These observations will be clarified in Sec. IV A.

A. Theoretical predictions

From the set of stochastic equation (5), we derive the Fokker–Planck equation for the probability distribution function, $p = p(\{x\}, \{v\})$ (where the symbol $\{\cdot\}$ has been introduced to denote all the space-components of the N particles),

$$\frac{\partial}{\partial t}p = -\mathbf{v}_i \cdot \nabla_{\mathbf{x}_i} p + \frac{1}{\tau}\left(\mathcal{I}_{ij} + \frac{\tau}{\gamma}\nabla_{\mathbf{x}_i}\nabla_{\mathbf{x}_j}U\right)\nabla_{\mathbf{v}_i} \cdot (\mathbf{v}_j p)$$
$$+ \frac{\nabla_{\mathbf{x}_i}U}{\tau\gamma} \cdot \nabla_{\mathbf{v}_i}p + \frac{v_0^2}{\tau}\nabla_{\mathbf{v}_i}\nabla_{\mathbf{v}_j}(\mathcal{D}_{ij}p), \tag{10}$$

where $\mathcal{I}_{ij}$ is the identity matrix and each element $\mathcal{D}_{ij}$ is a 2×2 symmetric matrix of the form

$$\mathcal{D}_{ij} = \delta_{ij}\begin{bmatrix} n_{y_i}^2 & -n_{x_i}n_{y_i} & 0 \\ -n_{x_i}n_{y_i} & n_{x_i}^2 & 0 \\ 0 & 0 & 0 \end{bmatrix}.$$

We remark that each $\mathcal{D}_{ij}$ is a non-diagonal matrix as a consequence of the complex noise structure in Eq. (5) and of the fact that $n_{x(y)}$ is a function of the particle velocity and position through Eq. (1). We

point out that Eq. (10) has the same form as the AOUP Fokker–Planck equation except for the diffusion-like term [i.e., the term containing $\mathcal{D}_{ij}$ in Eq. (10)]. However, in the AOUP equation, the non-diagonal matrix $\mathcal{D}_{ij}$ is replaced by a diagonal one, $\tilde{\mathcal{D}}_{ij}$, with components

$$\tilde{\mathcal{D}}_{ij} = \delta_{ij}\begin{bmatrix} 1 & 0 & 0 \\ 0 & 1 & 0 \\ 0 & 0 & 0 \end{bmatrix}.$$

We observe that $\tilde{\mathcal{D}}_{ij}$ can be obtained from $\mathcal{D}_{ij}$ just by replacing $n_{x(y)}^2$ and $n_x n_y$ by their averages, i.e., $\langle n_{x(y)}^2 \rangle = 1/2$ and $\langle n_x n_y \rangle = 0$, respectively (with the addition of an extra factor 2 needed for consistency between the parameters of the two models[73]). We remark that even in the simplified AOUP case, the solutions of Eq. (10) for $\tau > 0$ and generic potential are only known in the regime of small persistence, in particular, as an expansion in powers of $\tau\gamma$ around a Gaussian distribution.[68,71,75] On the contrary, in the case of interacting ABP, there are neither asymptotic nor approximated results for the probability distribution function of the velocity.

Being the general solution of Eq. (10) unknown, we will employ suitable approximations supported by numerical observations. In Fig. 2, we report $\langle|\mathbf{F}|\rangle$ and $\langle|\mathbf{v}|\rangle$ as a function of τ. In the small-persistence regime, $v_0 \approx \langle|\mathbf{v}|\rangle \gg \langle|\mathbf{F}|\rangle$, while in the large-persistence regime, the opposite relation holds, namely, $v_0 \approx \langle|\mathbf{F}|\rangle \gg \langle|\mathbf{v}|\rangle$, confirming the physical explanation mentioned before. Such an observation will be crucial in the following to derive approximate analytical solutions of $p(v)$.

1. Large persistence regime

Using the observation $v_0 \approx \langle|\mathbf{F}|\rangle \gg \langle|\mathbf{v}|\rangle$, holding in the large persistence regime, we have $\mathbf{n}_i \approx \nabla_i U$, and the diffusive matrix can be approximated as follows:

$$\mathcal{D}_{ij} \approx \delta_{ij}\frac{1}{v_0^2\gamma^2}\begin{bmatrix} (\nabla_{y_i}U)^2 & -\nabla_{y_i}U\nabla_{x_i}U & 0 \\ -\nabla_{y_i}U\nabla_{x_i}U & (\nabla_{x_i}U)^2 & 0 \\ 0 & 0 & 0 \end{bmatrix}.$$

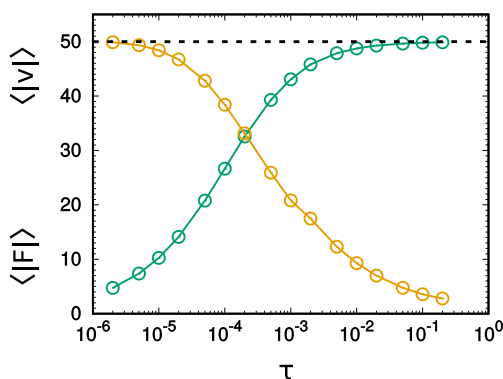**FIG. 2**. $\langle|\mathbf{v}|\rangle$ (yellow data) and $\langle|\mathbf{F}|\rangle$ (green data) as a function of τ. The black dashed line is drawn in correspondence to v_0 that is chosen as $v_0 = 50$ in the numerical simulations. The other parameters are $\varepsilon = \sigma = \gamma = 1$.

In the active solid phases, where the defects of the crystalline arrangement are negligible, the sum of the forces exerted by neighboring particles cancel out, and we can assume $\nabla_{x_i(y_i)}U = 0$. In other words, our approximation consists in replacing $\nabla_{x_i(y_i)}U$ with $\langle \nabla_{x_i(y_i)}U \rangle = 0$. This is true only in the high-density regime where we can approximate the gradient of the potential expanding the distance between neighboring particles around $\bar{r}$. Since $\langle \nabla_{x_i}U \nabla_{y_i}U \rangle = \langle \nabla_{x_i}U \rangle \langle \nabla_{y_i}U \rangle = 0$ and $\langle \nabla_{x_i}U \nabla_{x_i}U \rangle = v_0^2$, we obtain that $\mathcal{D}_{ij} \approx \tilde{\mathcal{D}}_{ij}$, proving that at very high density in the large persistence regime, the ABP velocity dynamics is well approximated by the AOUP dynamics. Even with this simplification, an exact solution is not known, and we shall employ an approximation for the many-body velocity distribution as follows:[61]

$$p(\{\mathbf{v}\}|\{\mathbf{x}\}) \propto \exp\left(-\frac{1}{2v_0^2} \sum_{ij} \mathbf{v}_i \cdot \boldsymbol{\Gamma}_{ij} \cdot \mathbf{v}_j \right). \tag{11}$$

$p(\{\mathbf{v}\}|\{\mathbf{x}\})$ is a multivariate Gaussian coupling the whole set of velocities through the space dependent matrix $\boldsymbol{\Gamma}_{ij}$. We remark that the prediction (11) is not the exact solution of the Fokker–Planck equation associated with the AOUP interacting dynamics, but it is a suitable approximation that works in the large persistence regime. This prediction has been tested in several cases, even under the action of external potentials.[55,76]

In the active solid phase, the matrix $\boldsymbol{\Gamma}_{ij}$, which depends on particles' relative positions, simplifies due to the hexagonal structure and the short-range nature of the interaction potential. Thus, the conditional probability distribution of $\mathbf{v}_i$ (i.e., knowing the velocity of the other particles) is given by Eq. (11) where the sum is restricted to the first six neighbors of the target particle. Integrating out all the velocity degrees of freedom except $\mathbf{v}_i$, we still obtain a Gaussian distribution with zero average, confirming the shape reported in Fig. 1 in the small persistence regime,

$$p(\mathbf{v}) \propto \exp\left(-\frac{\beta}{2}\mathbf{v}^2 \right), \tag{12}$$

where β is the variance of the distribution or the inverse of the kinetic temperature. Its exact expression as a function on the active force parameters will be derived in Sec. V.

2. Small persistence-regime

In the small persistence regime, the AOUP approximation is no longer valid, as numerically shown in Fig. 1. Indeed, according to the AOUP model, the shape of $p(v_x, v_y)$ should always be Gaussian (with asymptotic corrections) at variance with our numerical results obtained with ABP simulations. As shown in Fig. 2, we simplify the noise matrix assuming $v_0 \approx \langle |\mathbf{v}| \rangle \gg \langle |\mathbf{F}| \rangle$, obtaining

$$\mathcal{D}_{ij} \approx \delta_{ij}\frac{1}{v_0^2}\begin{bmatrix} v_y^2 & -v_y v_x & 0 \\ -v_y v_x & v_x^2 & 0 \\ 0 & 0 & 0 \end{bmatrix}. \tag{13}$$

The Fokker–Planck equation (10) with the matrix (13) (in the small τ limit) turns to be

$$\frac{\partial}{\partial t}p \approx -\mathbf{v}_i \cdot \nabla_{\mathbf{x}_i}p + \frac{1}{\tau}\nabla_{\mathbf{v}_i} \cdot (\mathbf{v}_j p)$$
$$+ \frac{\nabla_{\mathbf{x}_i}U}{\tau\gamma} \cdot \nabla_{\mathbf{v}_i}p + \frac{v_0^2}{\tau}\nabla_{\mathbf{v}_i}\nabla_{\mathbf{v}_j}[\mathcal{D}_{ij}p]. \tag{14}$$

Neglecting the term $\propto \nabla_{\mathbf{x}_i}U$ because the forces almost cancel out in the solid phase (and their modulus is smaller than the velocity modulus, as shown in Fig. 2), we can easily check that Eq. (14) admits a solution of the form

$$p(v_x, v_y) \propto \exp\left[-\frac{\alpha}{2}(|\mathbf{v}| - v_0)^2 \right]. \tag{15}$$

The shape of Eq. (15) corresponds to the Cartesian version of the velocity distribution shape numerically observed, i.e., Eq. (8).

V. THE KINETIC TEMPERATURE

In Fig. 3, we show the first two moments of the velocity modulus distribution as a function of τ, namely, $\langle |\mathbf{v}| \rangle$ and $\langle \mathbf{v}^2 \rangle$. The latter coincides by definition with the kinetic temperature of a system of ABP, and for this reason, we will denote $\langle \mathbf{v}^2 \rangle$ simply as "kinetic temperature" in the rest of this paper. For $\tau \lesssim 10^{-4}$, the system is in the small persistence regime [case (i)] and both $\langle |\mathbf{v}| \rangle$ and $\langle \mathbf{v}^2 \rangle$ are roughly constant with τ, being approximatively $\langle |\mathbf{v}| \rangle \approx v_0$ and $\langle \mathbf{v}^2 \rangle \approx v_0^2$. We recall that in this regime, the interparticle forces almost balance and the velocity displays the same statistical properties of the self-propulsion in such a way that the kinetic temperature does not display any τ-dependence. Upon increasing τ, the values of $\langle |\mathbf{v}| \rangle$ and $\langle \mathbf{v}^2 \rangle$ monotonically decrease reaching very small values. The more persistent is the particle motion, the slower it becomes, and as a consequence, the kinetic temperature decreases monotonically with τ. After a crossover regime occurring for $10^{-4} \lesssim \tau \lesssim 10^{-3}$, a clear power-law scaling with τ appears for $10^{-3} \lesssim \tau \lesssim 10^{-1}$ in both the moments. In particular, we have $\langle |\mathbf{v}| \rangle \sim v_0(\gamma\tau)^{-2/5}$ and $\langle \mathbf{v}^2 \rangle \sim v_0^2(\gamma\tau)^{-4/5}$, as clearly shown in Fig. 3. The validity of these scalings ceases approximatively at $\tau = 10^{-1}$, i.e., near the solid–hexatic transition. Starting from this value of τ, both $\langle |\mathbf{v}| \rangle$ and $\langle \mathbf{v}^2 \rangle$ decrease slower than $\sim\tau^{-2/5}$ and $\sim\tau^{-4/5}$ as the persistence time is increased without showing any clear power-law scaling with τ.

In what follows, we develop an exact, analytical prediction valid in the active solid-state for the kinetic temperature, which will explain the scaling with τ numerically observed, shedding light also
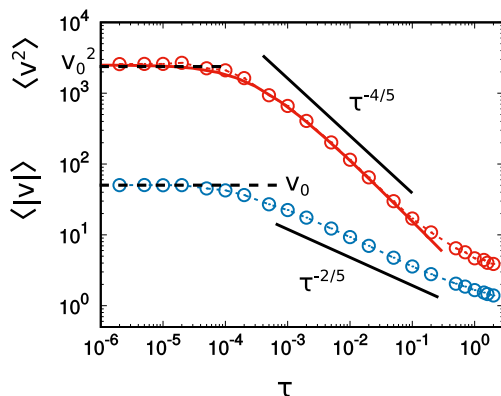
FIG. 3. $\langle \mathbf{v}^2 \rangle$ (red data) and $\langle |\mathbf{v}| \rangle$ (blue data) as a function of τ. The colored dashed lines are plotted as guides to the eye, while the solid red line represents the theoretical prediction, Eq. (20). Numerical simulations are realized with $v_0 = 50$ and $\epsilon = \sigma = \gamma = 1$.

on the role of the other parameters. Indeed, the periodicity of the almost-solid structure and, in particular, its hexagonal order suggests switching in the Fourier space to perform calculations.[38,60] As reported in the Appendix, the velocity correlation in the Fourier space reads

$$\langle \hat{\mathbf{v}}_\mathbf{q} \cdot \hat{\mathbf{v}}_{-\mathbf{q}} \rangle = \frac{v_0^2}{1 + \frac{\tau}{\gamma} \omega_\mathbf{q}^2}, \qquad (16)$$

where $\hat{\mathbf{v}}_q$ is the Fourier transform of the velocity vector $\mathbf{v}$ and $\mathbf{q} = (q_x, q_y)$ is a vector of the reciprocal Bravais lattice. The factor $\omega_\mathbf{q}^2$ has the following form:

$$\omega_\mathbf{q}^2 = -2K\left[\cos(q_x \bar{r}) + 2\cos\left(\frac{1}{2}q_x \bar{r}\right)\cos\left(\frac{\sqrt{3}}{2}q_y \bar{r}\right) - 3\right], \qquad (17)$$

where the dimensional constant K reads

$$2K = U''(\bar{r}) - \frac{U'(\bar{r})}{\bar{r}} \qquad (18)$$

and $\bar{r}$ is the average distance between neighboring particles. To obtain the variance of the velocity, we need to go back to the real space calculating the inverse Fourier transform in the origin as follows:

$$\langle \mathbf{v}^2 \rangle = \frac{v_0^2}{N^2} \sum_\mathbf{q} \frac{1}{\left(1 + \frac{\tau}{\gamma}\omega_\mathbf{q}^2\right)}. \qquad (19)$$

Taking the continuum limit in the $\mathbf{q}$-sum and accounting for the periodicity of the lattice, we restrict the integral to the first Brillouin zone,

$$\langle \mathbf{v}^2 \rangle \approx v_0^2 \mathcal{I}\left[\frac{\tau}{\gamma}\right], \qquad (20)$$

where

$$\mathcal{I}\left[\frac{\tau}{\gamma}\right] = \frac{\bar{r}^2}{|\mathcal{B}|} \int_\mathcal{B} d\mathbf{q} \frac{1}{\left(1 + \frac{\tau}{\gamma}\omega_\mathbf{q}^2\right)}, \qquad (21)$$

and $|\mathcal{B}|$ is the area of the Brillouin region associated with the hexagonal lattice. We remark that it is not possible to approximate $\omega_\mathbf{q}^2$ for small $\mathbf{q}$ truncating at the quadratic order since the integral diverges at $\mathbf{q} = 0$. To the best of our knowledge, Eq. (20) is the first analytical expression for the kinetic temperature of interacting self-propelled particles that does not require fitting parameters. We observe that our expression increases quadratically with v_0 in agreement with the previous results,[49] while the dependence on packing fraction and persistence time is contained in the integral $\mathcal{I}\left[\frac{\tau}{\gamma}\right]$. As shown in Fig. 3 (see the comparison between red points and the solid red line), Eq. (20) is in fair agreement with numerical data when the system attains solid configurations for $\tau \lesssim 10^{-1}$. On the one hand, $\mathcal{I}[0] \approx 1$ for small values of τ, while on the other hand, the numerical integration of $\mathcal{I}$ confirms both the crossover regime and the scaling $\sim(\tau/\gamma)^{-4/5}$ in the large persistence regime. For $\tau \gtrsim 10^{-1}$, Eq. (20) underestimates the values of $\langle \mathbf{v}^2 \rangle$ with respect to numerical data because for these values of τ, the structure of the system is no longer a solid without defects. Thus, a fundamental hypothesis behind the derivation of the prediction is violated, and thus, Eq. (20) is no longer valid. In particular, it has been already shown that, in the proximity of defects, active particles have kinetic energies

much larger than the ones in the absence of defects, as occurring in active solid configurations.[38] This is a clue to understanding why the decrease in $\langle \mathbf{v}^2 \rangle$ with τ in active hexatic phases is slower than the decrease for active solids. We remark that the kinetic temperature contains also the dependence on the packing fraction through the constant K [see Eqs. (17)–(19)]. Indeed, K is mainly determined by the second derivative of the potential calculated at $\bar{r}$ that is uniquely fixed by the packing fraction in any homogeneous configurations. The larger the ϕ, the larger the K and, thus, $\omega_\mathbf{q}^2$. Therefore, the growth of ϕ induces the decrease in the kinetic temperature through the non-linear derivatives of the function $U(\bar{x})$. The explicit dependence on the potential shape is in agreement with the previous studies based on temperature definitions derived in simpler cases, namely, a one-dimensional particle confined through an external potential.[54,55]

A. Higher-order moments and non-Gaussianity

Despite that the equilibrium-like Gaussian prediction is a good approximation of the velocity distribution, at least in the large persistence regime, even from Fig. 1(d), clear deviations from the Gaussian theory are evident in its tails. To get a quantitative analysis of the non-Gaussianity, we report the behavior of the higher-order moments in Fig. 4. In particular, we show the kurtosis of the v_x-distribution, namely, $\langle v_x^4 \rangle / \langle v_x^2 \rangle^2$. This observable is rather small (around ~1) in the small-τ regime as a result of the non-Gaussianity of the distribution [Fig. 1(c)]. On the contrary, in the Gaussian-like regime, for $\tau \gtrsim 10^{-3}$, the kurtosis shows just small departures from the Gaussian prediction corresponding to $\langle v_x^4 \rangle / \langle v_x^2 \rangle^2 = 3$. In particular, our numerical observations reveal that $\langle v_x^4 \rangle / \langle v_x^2 \rangle^2 \geq 3$, meaning that the tails of the distribution are a little fatter than the Gaussian prediction. Finally, for larger values of τ, i.e., for $\tau > 10^{-1}$ at the solid–hexatic transition point, the kurtosis abruptly increases, and the system departs from the Gaussian-like regime. As already mentioned, this is consistent with the occurrence of intermittency
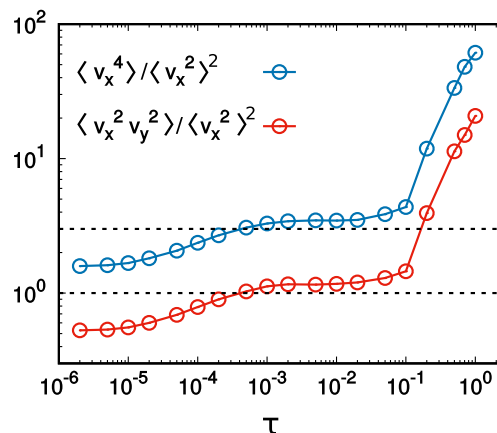
FIG. 4. $\langle v_x^4 \rangle / \langle v_x^2 \rangle^2$ (blue data) and $\langle v_x^2 v_y^2 \rangle / \langle v_x^2 \rangle^2$ (red data) as a function of τ. The colored solid lines are guides to the eye, while the dashed black lines are marked in correspondence to $\langle v_x^4 \rangle / \langle v_x^2 \rangle^2 = 3$ and $\langle v_x^2 v_y^2 \rangle / \langle v_x^2 \rangle^2 = 1$, i.e., at the expected values for a velocity following the Gaussian statistics. Numerical simulations are realized with $v_0 = 50$ and $\varepsilon = \sigma = \gamma = 1$.

phenomena in the hexatic phase[38] that manifest themselves also in high and non-Gaussian peaks in the time-trajectory of the single-particle kinetic energy. As a further confirmation, a similar scenario, consistent with the observation regarding the kurtosis, occurs for the observable, $\langle v_x^2 v_y^2 \rangle / \langle v_x^2 \rangle^2$. In particular, $\langle v_x^2 v_y^2 \rangle / \langle v_x^2 \rangle^2 \lesssim 1$ in the small persistence regime, 1 for regime with $10^{-3} \leq \tau \leq 10^{-1}$ (as expected in Gaussian regimes), and $\gtrsim 1$ when the hexatic phase occurs.

VI. DISCUSSION AND CONCLUSIONS

In this paper, we have studied the velocity properties of highly packed systems of self-propelled particles (active hexatic and solid phases) to understand the influence of the activity. A transition from Mexican-hat-like velocity distribution (i.e., peaked in the proximity of a circular crown with a radius larger than zero) to Gaussian-like velocity distribution is observed going from the small persistence to the large persistence time regime. Analyzing the velocity dynamics, we derive suitable approximations to predict the functional form of the probability distribution function of the velocities in both these regimes. Concerning the active solid, we derive by a Fourier-space method a theoretical expression for the variance of the velocity distribution, giving the kinetic temperature of ABP in this phase. Thus, on the one hand, we have derived new approximate analytical results concerning the velocity distribution of ABP particles holding both near and far from equilibrium, and on the other hand, we have provided the analytical expression for the active kinetic temperature in the solid phase.

At least in homogeneous solid configurations, the analytical expression for the kinetic temperature reported in this work increases quadratically with the swim velocity of the self-propelled particles (that is proportional to the Peclet number). This quadratic scaling has been also observed by means of different definitions of temperature, such as the active effective temperature.[50,52] Our expression of the kinetic temperature also displays a monotonic decrease as a function of the packing fraction in agreement with Ref. 49 where the effective temperature has been considered. Our results show that the kinetic temperature contains a strong dependence on the shape of the interacting potential in agreement with another temperature definition obtained in the case of a single-particle confined through an external potential.[54,55] Thus, the concavity of the potential plays a fundamental role not only for confined non-interacting active particles[76] but also for interacting systems, being relevant to determine the velocity variance (and, thus, the kinetic temperature) in both cases. While the kinetic temperature does not show a dependence on τ in the small persistence regime, a power-law decay with τ is numerically observed and theoretically predicted in the large persistence regime. We remark that our predictions are valid in the active solid-state while does not work where orientational and/or positional orders are broken (i.e., active hexatic and liquid state, respectively). In those cases, the occurrence of large non-Gaussianity and intermittency phenomena in the time-trajectory of the kinetic energy is consistent with the failure of the theoretical predictions.[38]

APPENDIX: THE KINETIC TEMPERATURE OF ACTIVE PARTICLES IN THE SOLID-STATE

To develop a prediction for the kinetic temperature of self-propelled particles in the active solid state, we shall employ two approximations to simplify the dynamics, Eq. (1). (i) The dynamics of each component of $\mathbf{f}_i^a$ is replaced by independent Ornstein–Uhlenbeck processes with equivalent persistence time, $\tau = 1/D_r$, and variance v_0^2 in such a way that $\langle |\mathbf{f}^a| \rangle = v_0$ consistently with the ABP model. (ii) Each particle oscillates around a node of a hexagonal lattice so that the total interparticle potential is approximated as the sum of quadratic terms. With these two assumptions, the original dynamics, Eq. (1), becomes

$$\dot{\mathbf{x}}_i(t) = \mathbf{f}^a(t)_i - \sum_j^{n.n} \frac{\nabla_i U(|\mathbf{x}_j - \mathbf{x}_i|)}{\gamma}, \tag{A1}$$

$$\tau \dot{\mathbf{f}}_i^a(t) = -\mathbf{f}^a(t)_i + v_0 \sqrt{2\tau}\, \boldsymbol{\xi}_i(t), \tag{A2}$$

where the sum involves the nearest neighbors of the lattice node i and the symbol ∇_i is the gradient with respect to $\mathbf{x}_i$. Introducing the displacement $\mathbf{u}_i$ of the particle i with respect to its equilibrium position, $\mathbf{x}_i^0$, namely,

$$\mathbf{u}_i = \mathbf{x}_i - \mathbf{x}_i^0, \tag{A3}$$

we obtain

$$\dot{\mathbf{u}}_i(t) = \mathbf{f}^a(t)_i + \frac{K}{\gamma} \sum_j^{n.n} (\mathbf{u}_j - \mathbf{u}_i), \tag{A4}$$

$$\tau \dot{\mathbf{f}}_i^a(t) = -\mathbf{f}^a(t)_i + v_0 \sqrt{2\tau}\, \boldsymbol{\xi}_i(t), \tag{A5}$$

with K being the strength of the potential in the harmonic approximation, i.e., $U \approx \frac{K}{2}(\mathbf{u}_j - \mathbf{u}_i)^2$, that explicitly reads

$$2K = \left(U''(\bar{r}) + \frac{U'(\bar{r})}{\bar{r}} \right),$$

where $\bar{r}$ is the lattice constant. Because of the linearity of the system, it is useful to switch to normal coordinates in the Fourier space representation,

$$\hat{\mathbf{u}}_{\mathbf{q}} = \frac{1}{N} \sum_i \mathbf{u}_i\, e^{-i\mathbf{q} \cdot \mathbf{x}_i^0}, \tag{A6}$$

$$\hat{\boldsymbol{\eta}}_{\mathbf{q}} = \frac{1}{N} \sum_i \boldsymbol{\eta}_i\, e^{-i\mathbf{q} \cdot \mathbf{x}_i^0}, \tag{A7}$$

where $\hat{\mathbf{u}}_{\mathbf{q}}$ and $\hat{\boldsymbol{\eta}}_{\mathbf{q}}$ are the Fourier transform of $\mathbf{u}$ and $\mathbf{f}^a$, respectively. The dynamics in the Fourier Space reads

$$\frac{d}{dt} \hat{\mathbf{u}}_{\mathbf{q}}(t) = -\frac{\omega_{\mathbf{q}}^2}{\gamma} \hat{\mathbf{u}}_{\mathbf{q}}(t) + \hat{\boldsymbol{\eta}}_{\mathbf{q}}, \tag{A8}$$

$$\tau \frac{d}{dt} \hat{\boldsymbol{\eta}}_{\mathbf{q}}(t) = -\hat{\boldsymbol{\eta}}_{\mathbf{q}} + v_0 \sqrt{2\tau}\, \hat{\boldsymbol{\xi}}_{\mathbf{q}}, \tag{A9}$$

02 May 2024 12:26:31

where

$$\omega_{\mathbf{q}}^2 = -2K\left[\cos(q_x\tilde{r}) + 2\cos\left(\frac{1}{2}q_x\tilde{r}\right)\cos\left(\frac{\sqrt{3}}{2}q_y\tilde{r}\right) - 3\right],$$

where $\mathbf{q} = (q_x, q_y)$ are vectors of the reciprocal Bravais lattice. Defining $\hat{\mathbf{v}}_{\mathbf{q}}$ as the Fourier transform of the velocity $\mathbf{v}$ that satisfies $\hat{\mathbf{v}}_{\mathbf{q}} = \frac{d}{dt}\hat{\mathbf{u}}_{\mathbf{q}}$, we can easily calculate the steady-state equal time correlations in the Fourier space, that is,

$$\langle \hat{\mathbf{v}}_{\mathbf{q}} \cdot \hat{\mathbf{v}}_{-\mathbf{q}} \rangle = \frac{2v_0^2}{1 + \frac{\tau}{\gamma}\omega_{\mathbf{q}}^2}. \tag{A10}$$

Equation (A10) is the final expression for the spatial velocity correlation in the Fourier space and corresponds to Eq. (16).

DATA AVAILABILITY

The data that support the findings of this study are available from the corresponding author upon reasonable request.

REFERENCES

[1] C. Bechinger, R. Di Leonardo, H. Löwen, C. Reichhardt, G. Volpe, and G. Volpe, Rev. Mod. Phys. **88**, 045006 (2016).

[2] M. C. Marchetti, J. F. Joanny, S. Ramaswamy, T. B. Liverpool, J. Prost, M. Rao, and R. A. Simha, Rev. Mod. Phys. **85**, 1143–1189 (2013).

[3] É. Fodor and M. Cristina Marchetti, Physica A **504**, 106–120 (2018).

[4] G. Gompper, R. G. Winkler, T. Speck, A. Solon, C. Nardini, F. Peruani, H. Löwen, R. Golestanian, U. B. Kaupp, L. Alvarez et al., J. Phys.: Condens. Matter **32**, 193001 (2020).

[5] C. Dombrowski, L. Cisneros, S. Chatkaew, R. E. Goldstein, and J. O. Kessler, Phys. Rev. Lett. **93**, 098103 (2004).

[6] J. Dunkel, S. Heidenreich, K. Drescher, H. H. Wensink, M. Bär, and R. E. Goldstein, Phys. Rev. Lett. **110**, 228102 (2013).

[7] H. Wioland, F. G. Woodhouse, J. Dunkel, and R. E. Goldstein, Nat. Phys. **12**, 341–345 (2016).

[8] S. Henkes, K. Kostanjevec, J. M. Collinson, R. Sknepnek, and E. Bertin, Nat. Commun. **11**, 1405 (2020).

[9] N. Sepúlveda, L. Petitjean, O. Cochet, E. Grasland-Mongrain, P. Silberzan, and V. Hakim, PLoS Comput. Biol. **9**, e1002944 (2013).

[10] S. Garcia, E. Hannezo, J. Elgeti, J.-F. Joanny, P. Silberzan, and N. S. Gov, Proc. Natl. Acad. Sci. U. S. A. **112**, 15314–15319 (2015).

[11] M. Basan, J. Elgeti, E. Hannezo, W.-J. Rappel, and H. Levine, Proc. Natl. Acad. Sci. U. S. A. **110**, 2452–2459 (2013).

[12] J. M. Nava-Sedeño, A. Voß-Böhme, H. Hatzikirou, A. Deutsch, and F. Peruani, Philos. Trans. R. Soc., B **375**, 20190378 (2020).

[13] D. Sarkar, G. Gompper, and J. Elgeti, arXiv:2006.04519 (2020).

[14] Y. Fily and M. C. Marchetti, Phys. Rev. Lett. **108**, 235702 (2012).

[15] I. Buttinoni, J. Bialké, F. Kümmel, H. Löwen, C. Bechinger, and T. Speck, Phys. Rev. Lett. **110**, 238301 (2013).

[16] M. E. Cates and J. Tailleur, Annu. Rev. Condens. Matter Phys. **6**, 219–244 (2015).

[17] G. Gonnella, D. Marenduzzo, A. Suma, and A. Tiribocchi, C. R. Phys. **16**, 316–331 (2015).

[18] Z. Ma, M. Yang, and R. Ni, Adv. Theory Simul. **3**, 2000021 (2020).

[19] L. Caprini, U. M. B. Marconi, and A. Puglisi, Phys. Rev. Lett. **124**, 078001 (2020).

[20] J. Stenhammar, D. Marenduzzo, R. J. Allen, and M. E. Cates, Soft Matter **10**, 1489–1499 (2014).

[21] J. T. Siebert, J. Letz, T. Speck, and P. Virnau, Soft Matter **13**, 1020–1026 (2017).

[22] F. Ginot, I. Theurkauff, F. Detcheverry, C. Ybert, and C. Cottin-Bizonne, Nat. Commun. **9**, 696 (2018).

[23] A. P. Solon, J. Stenhammar, M. E. Cates, Y. Kafri, and J. Tailleur, Phys. Rev. E **97**, 020602 (2018).

[24] M. N. van der Linden, L. C. Alexander, D. G. Aarts, and O. Dauchot, Phys. Rev. Lett. **123**, 098001 (2019).

[25] S. A. Mallory and A. Cacciuto, J. Am. Chem. Soc. **141**, 2500–2507 (2019).

[26] J. Grauer, H. Löwen, A. Be'er, and B. Liebchen, Sci. Rep. **10**, 5594 (2020).

[27] F. Jose, S. K. Anand, and S. P. Singh, arXiv:2004.01996 (2020).

[28] P. Chiarantoni, F. Cagnetta, F. Corberi, G. Gonnella, and A. Suma, J. Phys. A: Math. Theor. **53**, 36LT02 (2020).

[29] J. Bialké, T. Speck, and H. Löwen, Phys. Rev. Lett. **108**, 168301 (2012).

[30] A. M. Menzel and H. Löwen, Phys. Rev. Lett. **110**, 055702 (2013).

[31] G. Briand, M. Schindler, and O. Dauchot, Phys. Rev. Lett. **120**, 208001 (2018).

[32] J. U. Klamser, S. C. Kapfer, and W. Krauth, Nat. Commun. **9**, 5045 (2018).

[33] P. Digregorio, D. Levis, A. Suma, L. F. Cugliandolo, G. Gonnella, and I. Pagonabarraga, Phys. Rev. Lett. **121**, 098003 (2018).

[34] S. De Karmakar and R. Ganesh, Phys. Rev. E **101**, 032121 (2020).

[35] S. Paliwal and M. Dijkstra, Phys. Rev. Res. **2**, 012013 (2020).

[36] L. F. Cugliandolo, P. Digregorio, G. Gonnella, and A. Suma, Phys. Rev. Lett. **119**, 268002 (2017).

[37] P. Digregorio, D. Levis, L. F. Cugliandolo, G. Gonnella, and I. Pagonabarraga, arXiv:1911.06366 (2019).

[38] L. Caprini, U. M. B. Marconi, C. Maggi, M. Paoluzzi, and A. Puglisi, Phys. Rev. Res. **2**, 023321 (2020).

[39] R. Mandal, P. J. Bhuyan, P. Chaudhuri, C. Dasgupta, and M. Rao, Nat. Commun. **11**, 2581 (2020).

[40] J. Palacci, C. Cottin-Bizonne, C. Ybert, and L. Bocquet, Phys. Rev. Lett. **105**, 088304 (2010).

[41] L. Berthier and J. Kurchan, Nat. Phys. **9**, 310–314 (2013).

[42] D. Levis and L. Berthier, Europhys. Lett. **111**, 60006 (2015).

[43] Z. Preisler and M. Dijkstra, Soft Matter **12**, 6043–6048 (2016).

[44] S. K. Nandi and N. S. Gov, Soft Matter **13**, 7609–7616 (2017).

[45] G. Szamel, Europhys. Lett. **117**, 50010 (2017).

[46] S. K. Nandi and N. Gov, Eur. Phys. J. E **41**, 117 (2018).

[47] L. F. Cugliandolo, G. Gonnella, and I. Petrelli, Fluctuation Noise Lett. **18**, 1940008 (2019).

[48] S. Dal Cengio, D. Levis, and I. Pagonabarraga, Phys. Rev. Lett. **123**, 238003 (2019).

[49] I. Petrelli, L. F. Cugliandolo, G. Gonnella, and A. Suma, Phys. Rev. E **102**, 012609 (2020).

[50] A. Suma, G. Gonnella, G. Laghezza, A. Lamura, A. Mossa, and L. F. Cugliandolo, Phys. Rev. E **90**, 052130 (2014).

[51] I. Petrelli, P. Digregorio, L. F. Cugliandolo, G. Gonnella, and A. Suma, Eur. Phys. J. E **41**, 128 (2018).

[52] D. Loi, S. Mossa, and L. F. Cugliandolo, Soft Matter **7**, 10193–10209 (2011).

[53] S. Mandal, B. Liebchen, and H. Löwen, Phys. Rev. Lett. **123**, 228001 (2019).

[54] U. M. B. Marconi, A. Puglisi, and C. Maggi, Sci. Rep. **7**, 46496 (2017).

[55] L. Caprini, U. M. B. Marconi, and A. Puglisi, Sci. Rep. **9**, 1386 (2019).

[56] G. Szamel, Phys. Rev. E **90**, 012111 (2014).

[57] A. Puglisi, A. Sarracino, and A. Vulpiani, Phys. Rep. **709-710**, 1–60 (2017).

[58] T. F. Farage, P. Krinninger, and J. M. Brader, Phys. Rev. E **91**, 042310 (2015).

[59] G. S. Redner, M. F. Hagan, and A. Baskaran, Phys. Rev. Lett. **110**, 055701 (2013).

[60] L. Caprini and U. Marini Bettolo Marconi, Phys. Rev. Res. **2**, 033518 (2020).

[61] U. M. B. Marconi, N. Gnan, M. Paoluzzi, C. Maggi, and R. Di Leonardo, Sci. Rep. **6**, 23297 (2016).

[62] L. Berthier, E. Flenner, and G. Szamel, J. Chem. Phys. **150**, 200901 (2019).

[63] L. Caprini and U. Marini Bettolo Marconi, Soft Matter **15**, 2627–2637 (2019).

[64] E. Woillez, Y. Kafri, and N. S. Gov, Phys. Rev. Lett. **124**, 118002 (2020).

[65] C. Maggi, M. Paoluzzi, L. Angelani, and R. Di Leonardo, Sci. Rep. **7**, 17588 (2017).

[66] Y. Fily, J. Chem. Phys. **150**, 174906 (2019).

[67] L. Dabelow, S. Bo, and R. Eichhorn, Phys. Rev. X **9**, 021009 (2019).

[68] D. Martin, J. O'Byrne, M. E. Cates, É. Fodor, C. Nardini, J. Tailleur, and F. van Wijland, arXiv:2008.12972 (2020).

[69] L. Caprini and U. Marini Bettolo Marconi, Soft Matter **14**, 9044–9054 (2018).

[70] R. Wittmann, F. Smallenburg, and J. M. Brader, J. Chem. Phys. **150**, 174908 (2019).

[71] É. Fodor, C. Nardini, M. E. Cates, J. Tailleur, P. Visco, and F. van Wijland, Phys. Rev. Lett. **117**, 038103 (2016).

[72] C. Maggi, M. Paoluzzi, A. Crisanti, E. Zaccarelli, and N. Gnan, arXiv:2007.12660 (2020).

[73] L. Caprini, E. Hernández-García, C. López, and U. M. B. Marconi, Sci. Rep. **9**, 16687 (2019).

[74] S. Das, G. Gompper, and R. G. Winkler, New J. Phys. **20**, 015001 (2018).

[75] L. Caprini, U. M. B. Marconi, and A. Vulpiani, J. Stat. Mech.: Theory Exp. **2018**, 033203.

[76] L. Caprini, U. Marini Bettolo Marconi, A. Puglisi, and A. Vulpiani, J. Chem. Phys. **150**, 024902 (2019).

02 May 2024 12:26:31